Inorganic Chemistry

Article

pubs.acs.org/IC

Spectroscopic and Theoretical Studies of Ga(III)protoporphyrin-IX and Its Reactions with Myoglobin

Tyler B. J. Pinter,[†] Erin L. Dodd,[‡] D. Scott Bohle,[‡] and Martin J. Stillman*,[†]

[†]Department of Chemistry, The University of Western Ontario, London, Ontario, Canada

[‡]Department of Chemistry, McGill University, Montreal, Quebec, Canada

ABSTRACT: Ga(III)protoporphyrin-IX (Ga-PP) has been proposed as a model for the key interporphyrin interactions in malaria pigment. Unlike the paramagnetic parent iron heme derivatives, Ga-PP is readily soluble in methanol (MeOH). We report optical, mass spectroscopic, and theoretical results for Ga-PP as well as its reactions with myoglobin. UV−visible absorption and MCD spectroscopy show that Ga-PP exhibits a typical spectrum for a main group metal: a Q-band at 539 nm and a B band at 406 nm when dissolved in MeOH. We also report optical data for Zn(II)protoporphyrin IX (Zn-PP) dissolved in MeOH, which exhibits a Q-band at 545 nm and a B band at 415 nm. ESI mass spectral data for Ga-PP dissolved in MeOH show the presence of predominantly monomers, with smaller fractions of dimers [$(Ga\text{-}PP)_2$] and trimers. UV−visible and MCD absorption spectroscopy and ESI mass spectral data demonstrate the successful insertion of monomeric Ga-PP into apo-Mb. Ga-PP-Mb exhibits a B band at 417 nm and Q bands at 545 and 584 nm, which are all red-shifted from the free Ga-PP values. The calculated electronic structures and frontier molecular orbitals of Ga-PP, $(Ga\text{-}PP)_2$ and Zn-PP fit the previously reported trends in band energies and oscillator strengths as a function of molecular orbital energies. These new data can be applied to explain the experimentally observed optical spectroscopy. The observed Q-band energies are accounted for by calculated (HOMO−LUMO) gap of the frontier MOs, while the split in the two top occupied MOs accounts for the magnitude of the Q-band oscillator strength as well as the experimentally observed Q to B band energy separation. Although Ga-PP shares more spectroscopic properties with Zn-PP than it does with Fe(III)PPIX, the trivalent oxidation state allows this molecule to be used as a model for ferric hemes in heme proteins.

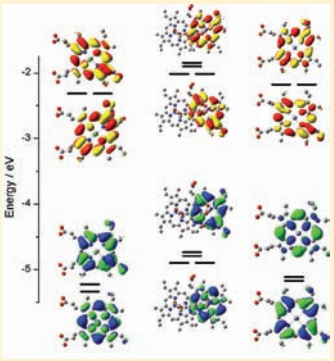

INTRODUCTION

The study of iron porphyrins is often complicated by its paramagnetism and resulting spin state ladder.[1] While these properties, and their influence on the heme redox potential, are often key to the biochemistry of this prosthetic group, it is unclear how much influence they have on heme aggregation and the subsequent interactions with heme binding proteins. A particular problem arises for the half filled shell in high-spin ferric hemes where the preferred out of plane, five coordinate geometry is accompanied by extensive aggregation and poor solubility, all of which makes characterization of ferric hemes by many solution methods, and particularly NMR spectroscopy, difficult, if not impossible.[2] Compounding the solution problem is the presence of charge transfer transitions, which complicate the optical spectrum making assignment of the underlying $\pi-\pi^*$ transitions hard but at the same time offering the power of fingerprinting in identifying oxidation, spin, and ligation status information.[3] While accurate theoretical calculations are necessary to be able to fully interpret the electronic structure of heme in proteins, calculations are also difficult due to the high/low spin duality of the heme iron. Therefore, diamagnetic noniron metalloporphyrins, where the central iron atom has been substituted with other metals, have garnered an increased interest in potential applications in biotechnological research. Two such applications that have used Ga(III)protoporphyrin IX (Ga-PP) are (i) as malarial pigment analogues[4] for drug development and (ii) as potential antibacterial agents.[5,6] With their filled d shell, size, and especially trivalency, Ga-PPs are considered to be good models for S = $^5/_2$ ferric hemes, especially for studies where the intermolecular heme−heme and heme−protein interactions need to be determined.

Ga-PP has been proposed as a possible hemozoin pigment model and, in particular in its dimerized form, it could benefit future drug discovery and development. The currently accepted mechanism for the activity of the malaria parasite involves the formation of the insoluble hemozoin pigment, which is a crystal of pure ferric heme.[7] The paramagnetic and charge transfer characteristics of heme make finding a suitable ferric heme analogue difficult. Compounding this is the increased insolubility that occurs when the heme aggregates to hemozoin.

Studies that Ga-PP could act as a potent antibacterial against gram-negative, gram-positive, and acid-fast bacteria were reported as early as 1999.[5] Since then there have been other reports of Ga-PP acting as an antibacterial agent against oral anaerobic bacterium *Porphyromonas gingivalis*.[6] It is proposed that gallium, which does not have an accessible Ga(III)/Ga(II) redox couple, would be incapable of participating in the electron transport roles that heme fulfills.[8] Ga-PP has also been shown to bind to heme containing proteins and enzymes when

Received: December 20, 2011
Published: February 28, 2012

dx.doi.org/10.1021/ic202731g | *Inorg. Chem.* 2012, 51, 3743−3753

it is included in the cellular growth medium of the Gram-positive bacteria *Enterococcus faecalis* which does not depend on heme for cell growth.[9] Clearly, future studies involving Ga-PP would greatly benefit from a detailed knowledge of the electronic structure of GaPP for comparison with the properties of ferric hemes; but this is currently unavailable to the best of our knowledge.

For each of these experiments, it is necessary to know the spectroscopic and aggregation properties of the Ga-PP heme model. In this Article, we describe spectroscopic and theoretical properties of Ga-PP and its dimer $(Ga\text{-}PP)_2$ in solution to provide specific data on the electronic structure of Ga-PP and compare these data with those of Zn-PP. In order to understand how Ga-PP might interact with heme proteins in vivo, we describe the in vitro reaction of Ga-PP with myoglobin, which is a well-defined model iron protoporphyrin IX binding protein. The electronic properties of Ga-PP are deduced from data obtained by UV−visible absorption and magnetic circular dichroism (MCD) spectroscopy, with stoichiometric and aggregation properties determined from electrospray ionization mass spectrometry (ESI-MS). Time-dependent DFT calculations of the electronic structures of the monomer and dimeric Ga-PP and the monomeric Zn-PP are reported for the first time. Finally, we compare the electronic properties of these models with the trends previously reported for a large series of synthetic porphyrins to illustrate the value of trends in assigning the optical spectrum.[10]

METHODS

Handling and Storage of Ga-PP. Ga-PP was synthesized by modifications to the method of Nakae et al.[11] and was stored in the dark at 4 °C. Solutions of Ga-PP(OMe) were prepared fresh for each experiment and kept at low concentrations (1 mM maximum). Sample measurements were taken as soon as possible after preparation.

Preparation of apo-Mb. Apo-Mb was prepared using the acid-butanone extraction method to remove the heme from a stock solution of 25 mg of holo-myoglobin dissolved in a minimum amount of 20 mM ammonium formate (pH 7.4).[12] Potassium ferricyanide was added (1 mg of $K_3[Fe(CN)_6]$/100 mg holo-Mb) to oxidize all iron present in the ferric form. The protein was separated from excess ferricyanide on a Sephadex G-25 (GE Healthcare) size exclusion column (7.8 cm^2 × 25 cm). The solution was acidified to pH 3 with concentrated formic acid before an equal volume of ice cold butanone was added to the protein solution and the mixture was shaken. The organic layer (deep red-brown), containing free heme, was allowed to separate from the aqueous layer containing the myoglobin. The extraction was repeated twice more until the organic layer no longer appeared colored and the aqueous layer was nearly colorless. The protein solution was exhaustively dialyzed against phosphate-buffered saline to remove excess butanone and stored at −80 °C until use.

Insertion of Ga-PP into apo-Mb. In total, 5 mg of Ga-PP was added to 10 mL of MeOH and refluxed until completely dissolved. Approximately a 3-fold molar excess of the pigment was added to a solution of 50 μM apo-myoglobin and stirred for 15 min at 4 °C. Separation of the holo protein from excess pigment was achieved using another Sephadex G-25 column (4.5 cm^2 × 10 cm) equilibrated with 20 mM ammonium formate buffer. Immediately prior to the ESI-MS experiments, the Ga-PP-Mb was thoroughly desalted using spin centrifuge buffer exchange filters (Amicon, 3000 MWCO).

Spectrophotometric Studies. Absorption spectra were recorded using dual-beam UV−visible absorption spectrophotometers (Cary 50 and Cary 500, Varian Canada). Steady state spectra of Ga-PP solutions and time-resolved spectra of pigment binding to the proteins were recorded to determine concentrations. Scan parameters: continuous scan; range 800−250 nm; scan rate = 600 nm/min; data interval = 1 nm; avg time = 0.1 s; spectral bandwidth = 1 nm.

CD spectra were measured on a Jasco 815 spectropolarimeter (Jasco, New Jersey), and MCD spectra were recorded by adding either an Oxford Instruments SM2 5.5 T superconducting magnet (Oxford Instruments, U.K.) (acquisition = 1 scan; $T_{cell} \sim 285$ K) or a 1.4 T permanent magnet (OLIS) (acquisition = 3 scans; $T_{cell} \sim 295$ K). Scan parameters were step scan; range 700−250 nm; data pitch = 1 nm; bandwidth = 0.5 nm; response = 1 s. MCD spectra were corrected for the zero field CD spectrum and zeroed at 700 nm before a 3 point fast Fourier transform filter was applied to smooth the data.

ESI-MS Data. A Bruker micrOTOF II ESI-TOF mass spectrometer (Bruker, Canada) operated in the positive ion mode was used for all ESI-MS measurements. Samples were infused into the spectrometer at a rate of 300 $\mu L\ h^{-1}$ using a microliter infusion pump. The instrument was calibrated with an external NaI/CsI standard solution. Data were processed using the Bruker DataAnalysis 4.0 software and deconvoluted using the Maximum Entropy deconvolution procedure. Parameters: rolling average = 2 × 0.5 Hz; end plate offset = −500 V; nebulizer = 2.0 bar; dry gas temp = 473 K; flow rate = 6.0 L/min; capillary voltage = 4500 V; capillary exit = 225 V; skimmer 1 = 42 V; hexapole = 23.0 V; hexapole rf = 425 Vpp.

DFT and TD-DFT Calculations. The Ga-PP and Zn-PP structures were created by replacement of the Fe in a heme structure from the Scigress Explorer (Ultra v7.7.0.49, Fujitsu) library database with Ga or Zn, respectively; the dimer was constructed from two of the Ga-PP molecules linked through the propionate side-chain in the manner shown by the crystal structure of hemozoin.[7] The structures underwent molecular modeling (MM3) and low level DFT (B88-PW91) geometry optimization using Scigress. Further ground state geometry optimizations were carried out with the Gaussian 03 program[13] by higher-level B3LYP/6-31G DFT calculations. The TD-DFT calculations for these optimized ground state geometries were then calculated as a separate experiment in Gaussian 03. In the case of Ga-PP and the dimer, the lack of Ga parametrization for DFT calculations required the use of a gallium pseudopotential (LANL2DZ "valence basis + pseudopotential" from https://bse.pnl.gov/bse/portal).[14,15]

RESULTS

Mass Spectrum of Solution State Ga-PP. Figure 1 shows the solution state ESI mass spectrum of Ga-PP freshly dissolved

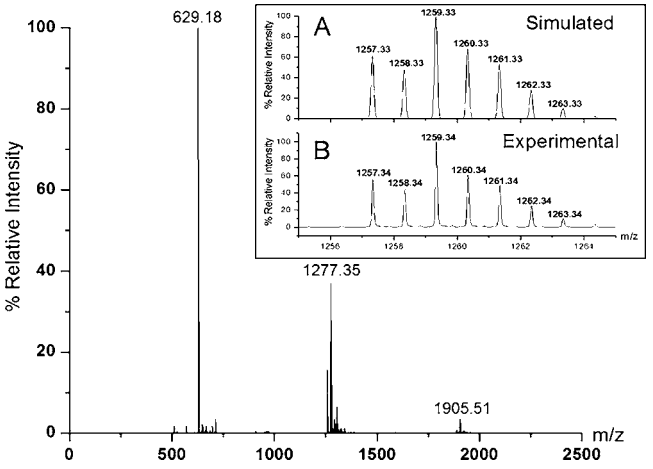

Figure 1. High-resolution ESI mass spectral data of Ga-PP (theoretical mass, 629.168 Da) and the $(Ga\text{-}PP)_2$ dimer in 100% MeOH. The inset box shows the simulated (A) and experimental (B) isotope patterns of the charged protonated dimer $(Ga\text{-}PP)_2{-}H^+$. The peak cluster at 1277.35 is representative of a water adduct of the protonated dimer. The peak cluster at 1905.51 is representative of the trimer adducted with two water molecules.

in 100% MeOH. When a fresh solution of Ga-PP is prepared in MeOH, Ga-PP exists as a number of species. The most

dx.doi.org/10.1021/ic202731g | Inorg. Chem. 2012, 51, 3743−3753

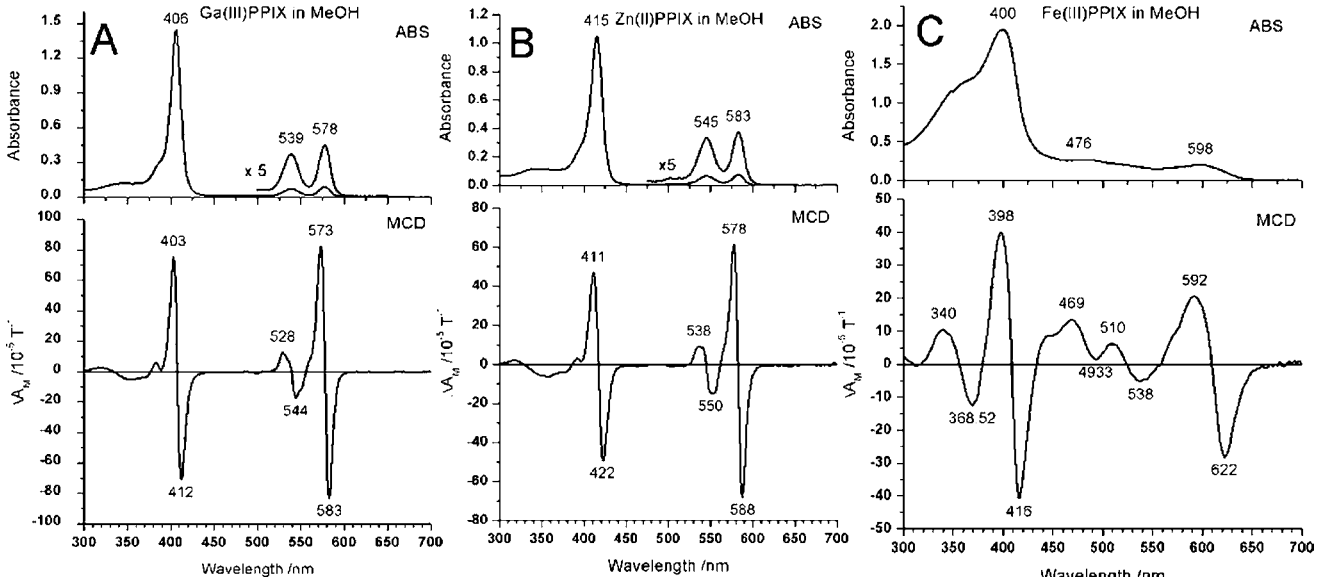

Figure 2. UV−visible absorption and MCD spectra at room temperature (298 K) of Ga-PP, Zn-PP, and ferric heme. (A) Ga-PP dissolved in MeOH, B-band at 406 nm, Q_{vib} at 539 nm, and Q_{00} at 578 nm. (B) Zn-PP in MeOH, B-band at 415 nm, Q_{vib} at 545 nm, and Q_{00} at 583 nm. (C) Ferric heme dissolved in MeOH, B-band at ∼400 nm, and Q_{00} at ∼600 nm. The MCD spectra of each PPIX show pseudo *A*-terms centered on the B, Q_{vib}, and Q_{00} bands.

prominent observed species are the monomer Ga-PP and the dimer $(Ga\text{-}PP)_2$ for which peaks are clearly observed, as well as a very small population of trimer $(Ga\text{-}PP)_3$. The calculated monoisotopic masses are Ga(III)PPIX $(C_{34}H_{32}O_4N_4Ga)^+$, 629.1674 Da; $(Ga\text{-}PP)_2$ $(C_{68}H_{63}O_8N_8Ga_2)^+$, 1257.3280 Da; and $(Ga\text{-}PP)_3$ $(C_{102}H_{94}O_{12}N_{12}Ga_3)$, 1885.4876. Each of these masses is observed also with water adducts (+ 18.01 Da). With the dimer, the most prominent species is the dimer with a single water adduct; while the trimer is adducted by two waters. This may indicate a coordination or trapping of H_2O sandwiched between the rings as the molecules aggregate. The inset in Figure 1 shows the calculated (A) and experimental (B) isotopic pattern for the protonated dimer.

UV−Visible Absorption Spectroscopy of Ga(III)PPIX, Zn(II)PPIX, and Fe(III)PPIX. Figure 2 shows the UV−visible absorption and MCD spectra of Ga-PP, Zn-PP, and ferric heme in MeOH. The spectrum of Ga-PP in MeOH (Figure 2A) is typical of a monomeric species and does not exhibit characteristics of aggregation or dimerization (wide bandwidths, multiple band peaks). The spectral bands can be accounted for based on the standard spectroscopic theory of porphyrins that identify the main bands as the Q-band and its vibronic band and the intense B-band. The B-band maximum for Ga-PP is at 406 nm, the Q_{vib} is at 539 nm, and Q_{00} is at 578 nm. The spectrum for Zn-PP in MeOH (Figure 2B) shows a strong resemblance to that of the Ga-PP with the a red-shifted B-band at 415 nm, Q-bands at 545 nm (Q_{vib}) and 583 nm (Q_{00}); while the ferric heme spectrum (Figure 2C) is markedly different with the B-band at 400 nm, an intense shoulder blue of the Soret band, and then multiple absorption bands through the visible region that are characteristic of charge transfer overlaying the Q-band at approximately 600 nm (Q_{00}).

The MCD spectra can be used to assign and confirm the origins of the visible absorption transitions because we expect MCD *A*-terms for the main group metals, while for ferric hemes pseudo *A*-terms, for the Q and B bands. Ga-PP shows sharp crossovers centered on the 578 nm (Q_{00}) and 407 nm (B or Soret) bands, while the Q_{vib} at 536 nm is skewed, likely the result of an overlapping transition from the small amount of dimer in solution. Zn-PP shows almost identical MCD spectroscopy to that of the Ga-PP, though the inflection points are not as sharp, the Q_{00} at 579 nm and the B at 416 nm are clear. The Q_{vib} at 441 nm is again slightly broadened by an overlapping transition. The UV regions of the two spectra look identical with small troughs on the blue side of the Soret bands and a broad band in the 300 nm region. Ferric heme shows a markedly different MCD spectrum from the other two molecules. With at least five well-defined transitions assignable and multiple others overlapping, the spectrum serves to show the complexity in ferric heme optical spectroscopy due to the additional charge transfer bands overlapping the $\pi-\pi^*$ bands of the ring.

ESI-Mass Spectral Data of Ga-PP-Mb. ESI mass spectral data of porphyrin protein reactions provide information regarding (i) the number of porphyrin rings associated with the protein; (ii) the state of bound porphyrins, (does the protein bind one or two rings); (iii) the structure of the protein (the percentage of protein that is folded or denatured after binding the ring); and (iv) an approximation of the relative populations of multiple porphyrin-loaded states in solution (relatively how much apo, PP-Mb, $(PP)_2$-Mb, etc.). The mass spectrum (Figure 3A) shows that the major charge states match the charge states for holo-Ga-PP-Mb monomers. The deconvoluted mass spectrum shown in Figure 3B shows masses that correspond to apo-Mb (16 952 Da), Ga-PP-Mb (17 581 Da), and a small fraction of $(Ga\text{-}PP)_2$-Mb (18 211 Da). Confirmation of the interpretation of the ESI-mass spectral data that myoglobin bound the Ga-PP in a structurally significant location was obtained using UV−visible absorption and MCD spectroscopy.

Spectroscopy of Ga-PP Bound to Myoglobin. The UV−visible and MCD spectroscopy of the myoglobin bound Ga-PP; Figure 4A shows a strongly red-shifted Soret band that is characteristic of M-PPIXs that are bound to Mb compared to their free solution spectra.[16] The MCD spectrum supports the results from the ESI-mass spectral data showing that there

dx.doi.org/10.1021/ic202731g | *Inorg. Chem.* 2012, 51, 3743−3753

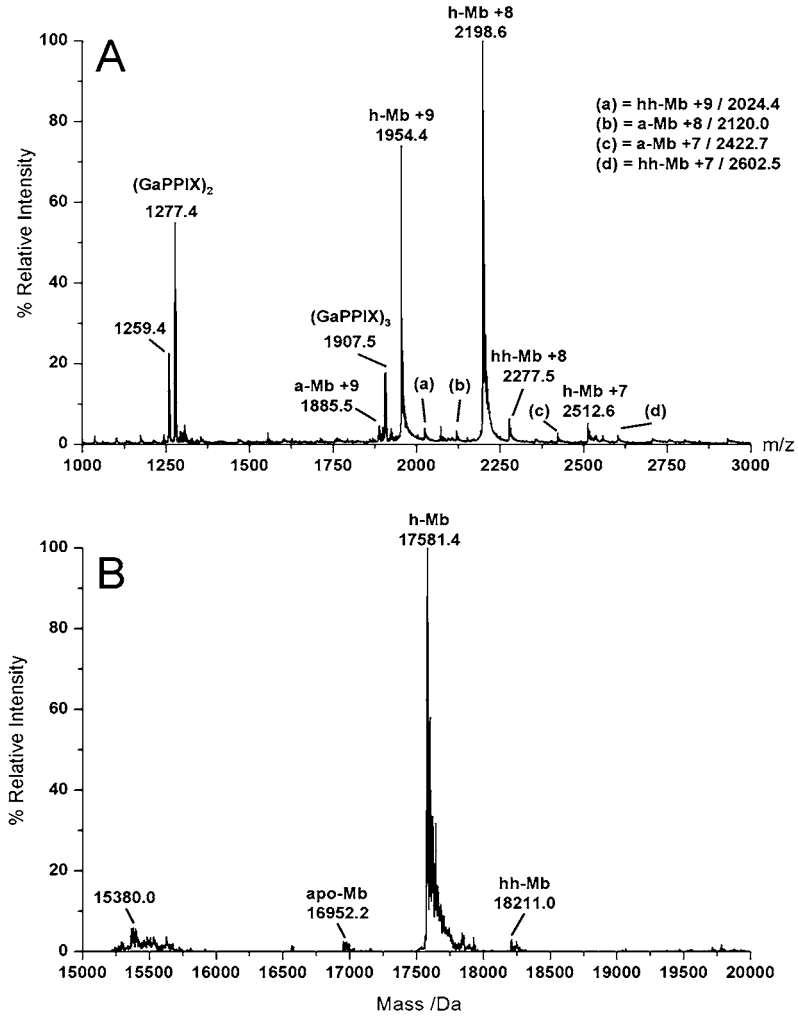

Figure 3. ESI mass spectral data of Ga-PP bound to myoglobin. (A) The charge state data. The data show that the myoglobin remains folded when Ga-PP binds. The notations used are $(Ga\text{-}PP)_2$, free dimer; a-Mb, apo myoglobin; $(Ga\text{-}PP)_3$, free trimer; h-Mb, holo myoglobin bound to Ga-PP; hh-Mb, holo myoglobin bound to dimer $(Ga\text{-}PP)_2$. Charge states are indicated. (B) The annotated deconvoluted data indicating the mass of the apo Mb, Ga-PP-Mb, and $(Ga\text{-}PP)_2$-Mb.

remains some free, unbound Ga-PP. This is indicated by the shoulders present in the MCD spectrum most notably on the MCD B-band, despite size exclusion separation of unbound pigment from protein. Attempts to purify the myoglobin bound pigment from this excess pigment in solution were unsuccessful due to a temperature-dependent instability. There exists an equilibrium between myoglobin bound monomer, solution state Ga-PP monomer, solution state Ga-PP dimer, and precipitated Ga-PP dimer; and soon after the Ga-PP-Mb is separated from the unbound pigment using size exclusion chromatography, the Ga-PP begins to form dimers and precipitates. Rapid measurements are required to observe the intact Ga-PP-Mb. The precipitation takes place over a couple of hours. The band at 650 nm is probably charge transfer of His to Ga^{3+}; and, as such, will show no change in angular momentum and not appear in the MCD spectrum. A very weak band in this region is also seen in this region in the spectrum of Ga-PP dissolved in pyridine.

The optical spectra of Ga-PP in pyridine solution are provided as a reference as the coordination of pyridine to the metal closely matches that of the proximal histidine in myoglobin. These results (Figure 4B) show that the B band shifts 12 nm to 418 and Q bands red shift to 546 and 590 nm compared to the free Ga-PP monomer in MeOH (Figure 2). The close similarity between the Ga-PP-Mb and Ga-PP dissolved in pyridine would suggest that the Ga^{3+} is coordinated to a single nitrogen donor (His or pyridine) and water or an anion. Table 1 below summarizes all of the observed measured MCD and UV−visible absorption transitions.

TD-DFT Calculation of Ga-PP, $(Ga\text{-}PP)_2$, and Zn-PP. To corroborate our assignment of the UV−visible absorption and MCD spectra of the Ga-PP, we carried out TD-DFT calculations for the Ga-PP. TD-DFT calculations involving Ga^{3+} are uncommon enough as to limit the availability of Ga^{3+} parameters, which required us to use a pseudopotential for the Ga atoms (see Methods for details). Using data extracted from the TD-DFT calculations, we constructed energy level diagrams for HOMO − 5 to LUMO + 5 for the three porphyrin systems (Figure 5). We have included the calculation for Zn-PP as a model of the PPIX $\pi-\pi^*$ transitions. Using these data, we were able to compare and contrast the findings for the monomer and the dimer with data already calculated and reported previously for a range of synthetic Zn porphyrin complexes.[10]

A key feature of the electronic structure of the monomeric protoporphyrin IX ring is that the effect of the asymmetry of

dx.doi.org/10.1021/ic202731g | Inorg. Chem. 2012, 51, 3743−3753

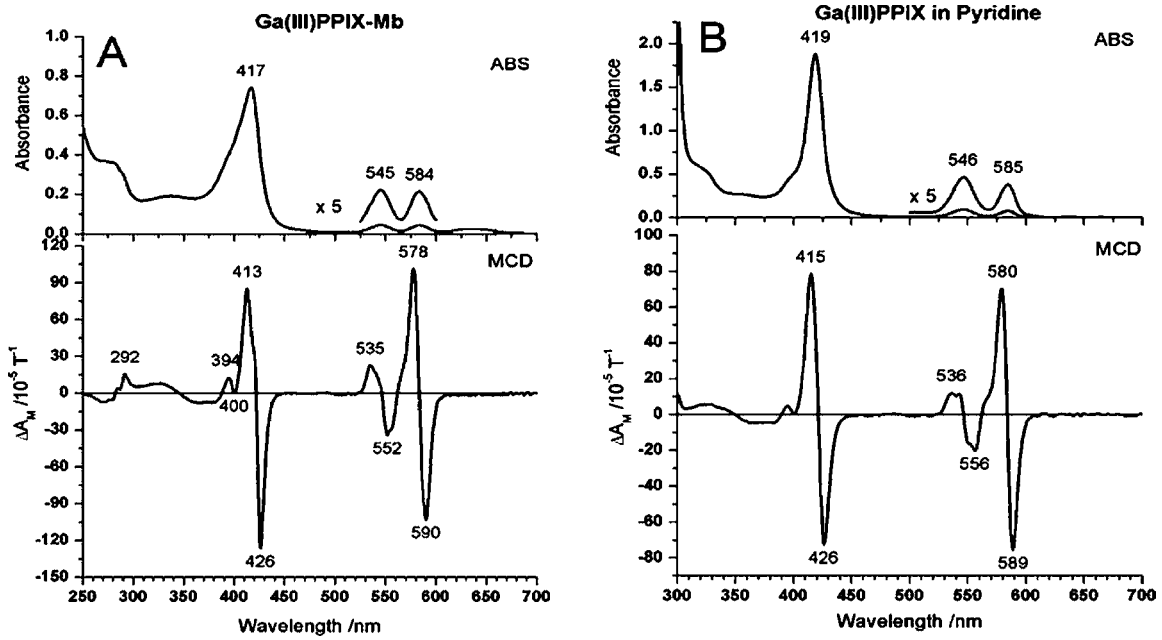

Figure 4. UV−visible absorption and MCD spectra of free Ga-PP and Ga-PP bound to myoglobin. (A) Spectra of the holo Ga-PP myoglobin immediately following excess pigment removal with size exclusion chromatography. (B) Ga-PP dissolved in pyridine as a model of the histidine coordination expected when bound to myoglobin.

Table 1. Summary of UV−Visible Absorption Band Maxima and Observed MCD peaks (+) and Troughs (−) in Nanometers (nm) of All Presented Optical Data[a]

	Zn(II)PPIX in MeOH					
	B/nm		Q_{vib} /nm		Q_{00} /nm	
ABS	415 (24 100 cm^{-1})		545 (18 350 cm^{-1})		583 (17 150 cm^{-1})	
MCD	+411	−422	+538	−550	+578	−588
	Ga(III)PPIX in MeOH					
	B		Q_{vib}		Q_{00}	
ABS	406 (24 630 cm^{-1})		539 (18 550 cm^{-1})		578 (17 300 cm^{-1})	
MCD	+403	−412	+526	−544	+573	−583
	Fe(III)PPIX in MeOH					
	B		Q_{vib}		Q_{00}	
ABS	400		CT[b]		607[c]	
MCD	+398	−416	CT[b]	CT[b]	+592	−622
	Ga(III)PPIX Pyridine					
	B		Q_{vib}		Q_{00}	
ABS	419		546		585	
MCD	+415	−426	+536	−556	+580	−589
	Ga(III)PPIX-Mb					
	B		Q_{vib}		Q_{00}	
ABS	417		545		584	
MCD	+413	−426	+535	−552	+578	−590

[a]Also provided are the band maxima in wavenumbers (cm^{-1}) for comparison to the energies determined from the TD-DFT calculations. [b]Q_{vib} for FePPIX is convoluted by charge transfer bands (CTB) that overlay the Q_{vib} transition. [c]Q-band was calculated by averaging the MCD peak to trough wavelengths.

the peripheral groups is primarily observed below the top two occupied MOs, the pair of split HOMOs of Gouterman's model, Figure 5A. Thus, MOs 157 and 158 for Ga-PP and 162 and 163 for Zn-PP are almost identical in distribution to the MOs of the symmetric Zn-porphyrins reported by us previously. The influence of the extensive peripheral substitution is only seen over 1 eV lower in energy. Similarly, the two lowest unoccupied MOs, the pair of nominally degenerate LUMO orbitals of Gouterman's model, also are reproduced unscathed by the presence of the two propionic side chains and vinyl groups. The influence of these peripheral substituents is seen at LUMO + 3 and above (162, 163, and 164 for Ga-PP and 167, 168, and 169 for Zn-PP). So for these two porphyrins, it is clear that the electronic structure is dominated by the four orbitals of Gouterman's model. The influence of the splitting of near-degenerate HOMO and LUMO pairs on the optical spectroscopy was first developed by Michl.[17] As we have noted already, the optical spectra resemble main group, symmetric porphyrins which clearly arise from the unusual presence of such symmetric highest occupied and lowest unoccupied MOs. The value of studying the Zn-PP is in determining the electronic structure in the absence of the many charge transfer states of heme. The isosurface diagrams in Figure 5, coupled with the orbital energies, are invaluable in illustrating the electronic rigidity of the 18 π electron aromatic ring in determining the underlying electronic properties of the PPIX ring. The fact that the peripheral substituents exert electronic influence only below HOMO − 2 and above LUMO + 3 suggests that these substituents have a structural role rather than an electronic role in the function of heme proteins.

The central set of data in Figure 5B shows that the energies of the highest occupied and lowest unoccupied MOs for $(Ga\text{-}PP)_2$ mirror the monomeric Ga-PP. The $(Ga\text{-}PP)_2$ dimer represents an interesting case: the arrangement of the dimer molecular orbital structure should follow as a simple extension of the monomer. That is, we would expect MOs of equal energy for the two sets of two HOMO and two LUMO. In fact, there is a splitting of the expected degeneracy likely due to the fact that the protoporphyrin rings are not coplanar and the optimized geometry for the linked dimer resembles an open clamshell. The four highest occupied MOs (305−308) exhibit the electronic distribution and nodal planes for an 18 π aromatic ring of a simple, symmetric ring. Indeed, the MOs are strongly

dx.doi.org/10.1021/ic202731g | Inorg. Chem. 2012, 51, 3743−3753

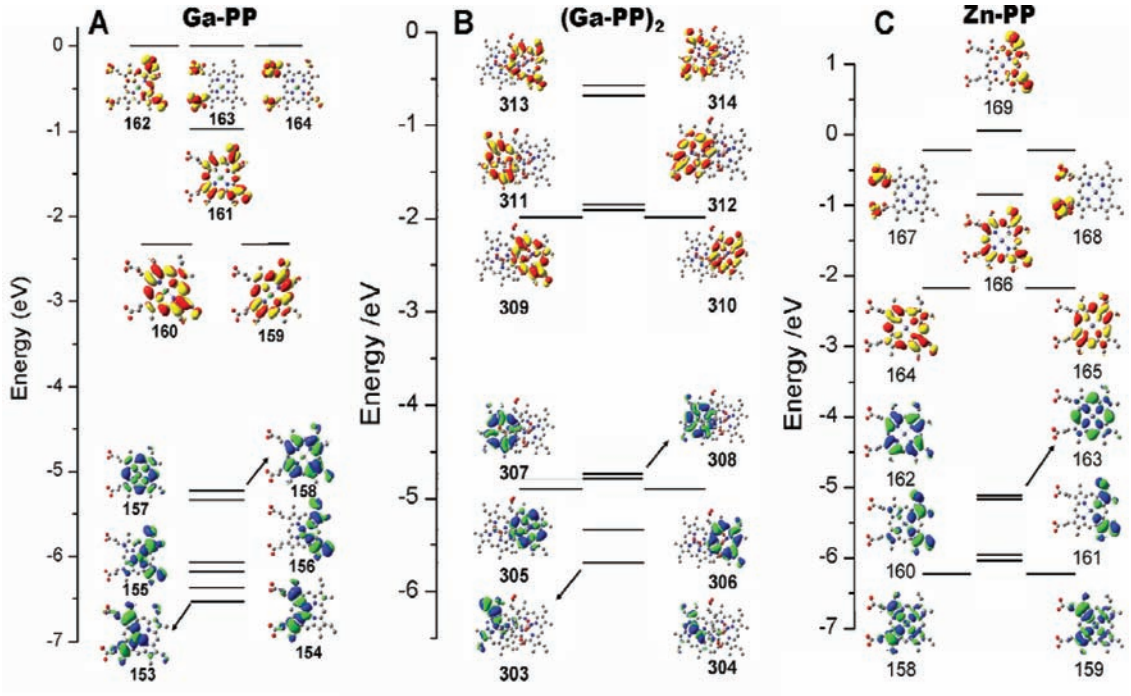

Figure 5. Energy level diagrams for (A) Ga-PP-OH, (B) the dimer $(Ga\text{-}PP)_2$, and (C) Zn-PP. Shown are the energies and molecular orbital surfaces for the top five occupied MOs (green and blue phases) and the lowest five unoccupied MOs (red and yellow phases). Hydrogens have been omitted from structures for clarity. The lowest shown molecular orbital for Ga-PP is HOMO − 5 at 153, for $(Ga\text{-}PP)_2$ is HOMO − 5 at 303, and for Zn-PP is HOMO − 5 at 158.

localized on each ring and not delocalized across both rings. This is undoubtedly due to the mode of dimerization in which the propionic side chain acts as the "leash" for the second ring. As the MOs for the isolated rings show, there is little delocalization from the 18 π ring on to the periphery. The lowest unoccupied MOs also mirror their monomeric models. The first four are 18 π-ring based. The peripheral effects of the vinyl side chains being the next highest at 311−314. The calculation of the optical spectrum (TD-DFT) shows that now there are interactions between the two rings, and the spectral properties will be a superposition of multiple transitions.

Recently we have determined a crystal structure of a Ga(PPIX) dimer which does not have coplanar protoporphyrin rings are also not coplanar in the solid state (data not published). The minimized DFT structure used in this work also shows a noncoplanar orientation of the two rings, Figure 6. This is likely a result of the presence of very different peripheral substituents, the vinyl and propionic side chains.

Upon closer inspection of the excited state transitions, we can observe the complexity that these skewed dimers introduce to the theoretical excited states. In the case of the monomer, as shown in Figure 7 below, the excited states closely follow Gouterman's description and Michl's extension: the two calculated transitions in the Q-band region both involve interactions between the pair of HOMOs and pair of degenerate LUMOs.

Compared to the dimer, shown in Figure 8, the Q-band region calculated excited states are a reasonably simple mixture of combinations of one-electron transitions. In fact, even though the MO surfaces of the dimer show that each MO is largely localized on a single ring (Figure 5), there exist a number of interactions between these rings that generate the optical transitions. This means that though the rings are tied through the propionate bridge, the two MOs are delocalized across both rings.

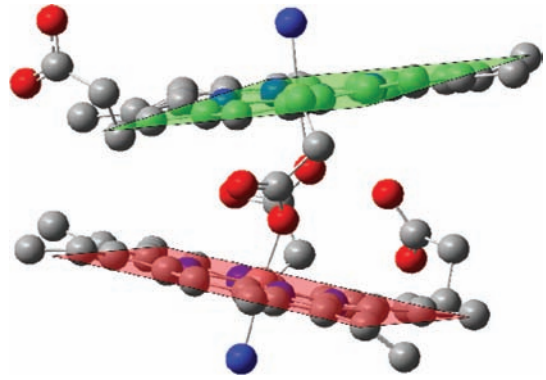

Figure 6. Optimized geometry for the $(Ga\text{-}PP)_2$ dimer as a dihydrate. The approximate planes of the two protoporphyrin rings are highlighted showing that the ring planes are noncoplanar and that the molecular structure is, therefore, asymmetric.

TD-DFT calculations were used to calculate the optical spectrum for two monomers and the dimer. Of interest are the contributions to the Q bands in each complex as this band fixes the electrochemical and optical properties of the heme proteins. For the two monomers, we find as expected that the Q-band are fairly pure, with a slight splitting of the S_1 Q state arising from the lack of symmetry. The HOMO−LUMO gap essentially ensures that the major contributions to this state are from the HOMO "pair" and the LUMO "pair" for Michl's system. Figure 7 illustrates the contributions for Ga-PP and Zn-PP. We return below to the value of connecting the Q and B band energies with the energies of the MOs in assigning spectra of novel porphyrins.

dx.doi.org/10.1021/ic202731g | Inorg. Chem. 2012, 51, 3743−3753

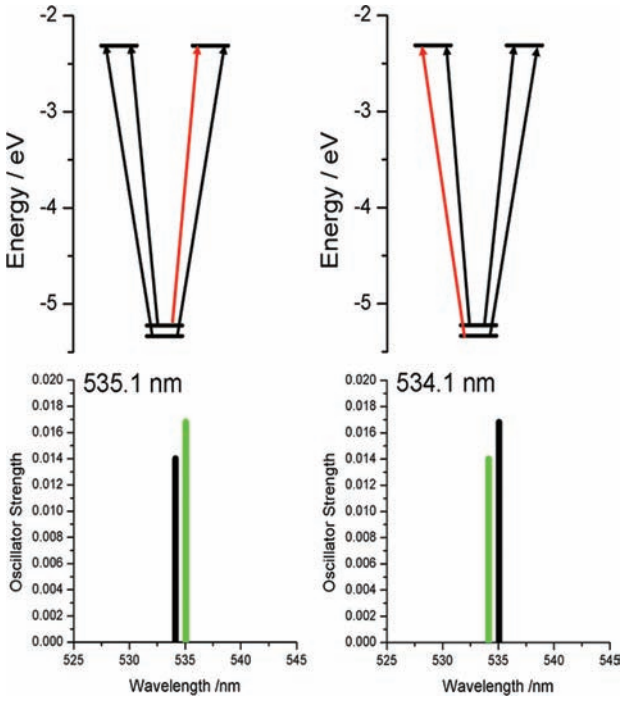

Figure 7. Contributions of molecular orbitals to excited states in the Q-band region for the Ga-PP from TD-DFT. Arrows in red indicate a negative phase contribution to the excited state. The highlighted green absorbance on the bottom results from the sum of the transitions shown in red (−) and black (+) above.

We turn now to the spectral properties predicted for $(Ga\text{-}PP)_2$, Figure 8. As noted above, there are four MOs in each of the HOMO region and LUMO regions, Figures 5 and 13. We can associate these MOs with each ring and then identify inter-ring transitions that lie in the Q-band region. In Figure 8 we break down the contributions to each of the absorption bands according to the initial and terminal MOs. Dashed lines indicate ring to ring transfers. Table 2 provides the phase and coefficients of the calculated absorption band composition. It is clear that even though the MOs were reasonably localized on the two rings, transfer between the rings occurred (blue arrows in Figure 8) and we suggest that this results in the typical dimer-spectrum observed for porphyrins, namely, band broadening and doubling. Because we were unable to obtain good optical spectra of the dimer, the theoretical calculations can only suggest what might be observed.

Finally, in order to evaluate the accuracy and validity of the TD-DFT calculations reported here, we compared the energies of the highest occupied and lowest unoccupied molecular orbitals (Gouterman's four-orbital model) with the results from calculations for a range of synthetic porphyrins that were previously reported by Mack and co-workers.[10] By inspection, the energy levels of the Ga-PP and Zn-PP matched closely with the simplest porphyrin (Zn−P in Figure 9) than with more complex synthetic Zn porphyrins.

Figure 10, which shows the experimentally observed Q-band energy as a function of the HOMO−LUMO gap for Ga-PP, $(Ga\text{-}PP)_2$, and Zn-PP shows that the larger HOMO−LUMO gaps of these simpler porphyrins generally result in a higher energy Q-band. Ga-PP and Zn-PP have a gap of 23 200 and 23 700 cm^{-1}, respectively, and Q-band energies of 17 300 and 17 150 cm^{-1}, respectively.

Another application of the series of Gouterman's four orbitals from Figure 9 can be drawn from Figure 11 where the data for the oscillator strengths of the Q-band for a wide range of porphyrins and phthalocyanines are plotted against the

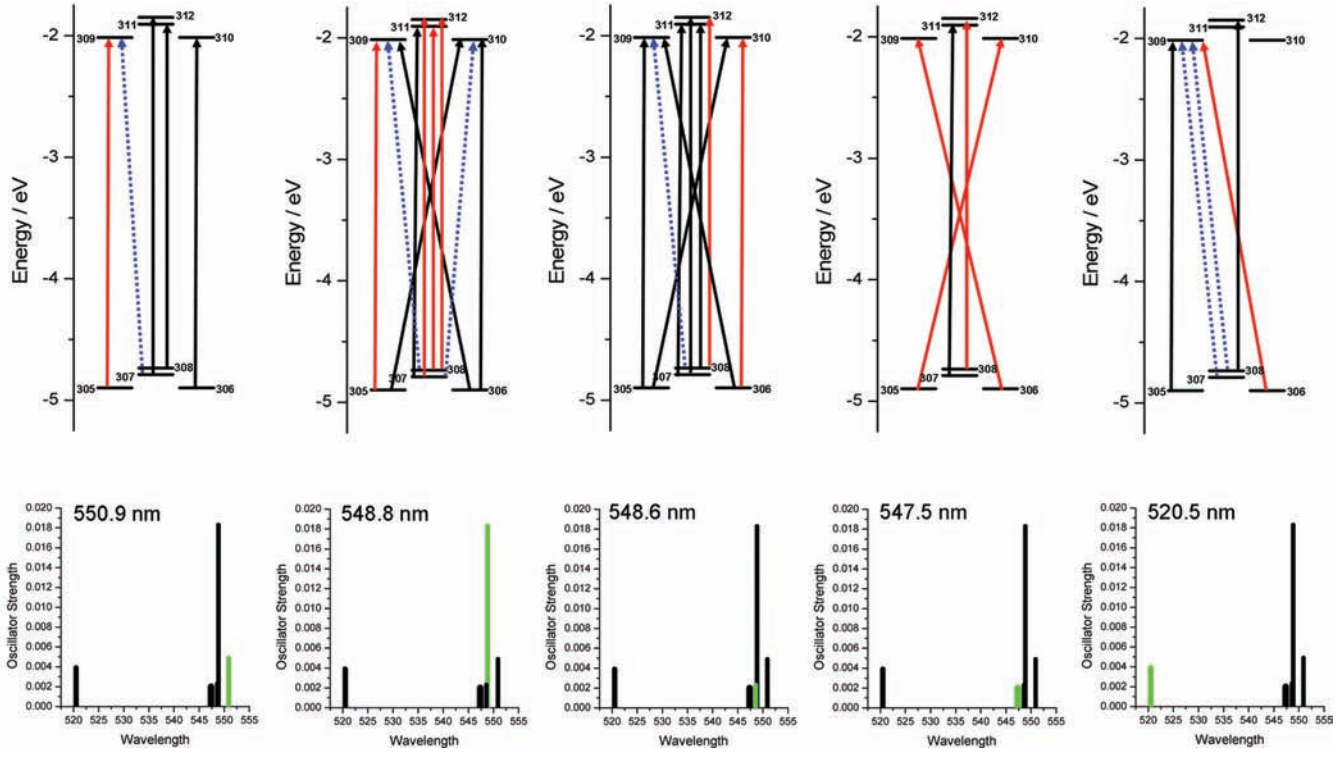

Figure 8. Individual contributions of molecular orbitals to the excited states in the Q-band region for the $(Ga\text{-}PP)_2$ dimer. The highlighted green absorption transition of the set of transitions that comprise the Q-band results from the sum of transitions in the energy level diagram directly above. Arrows in red indicate a negative contribution to the excited state. Dashed arrows are indicative of ring−ring molecular orbital interactions.

dx.doi.org/10.1021/ic202731g | Inorg. Chem. 2012, 51, 3743−3753

Table 2. Summary of Calculated Excited State Transitions of GaPP and $(GaPP)_2$ Determined from TD-DFT Calculation[a]

		GaPP			
state 1	535.06 nm	f = 0.0168	state 2	534.12 nm	f = 0.0140
157 → 159		0.1151	157 → 159		−0.4748
157 → 160		0.4695	157 → 160		0.1175
158 → 159		0.5142	158 → 159		0.1200
158 → 160		−0.1235	158 → 160		0.5087
		$(GaPP)_2$			
state 1	550.86 nm	f = 0.0049	state 2	548.80 nm	f = 0.0183
305 → 309		−0.1519	305 → 309		−0.2408
306 → 310		0.1666	305 → 310		0.3191
307 → 309		−0.1988	306 → 309		0.3256
307 → 312		0.4138	306 → 310		0.2417
308 → 311		0.4678	307 → 310		0.1051
			307 → 311		0.2164
			307 → 312		−0.1415
			308 → 309		0.1666
			308 → 311		−0.1361
			308 → 312		−0.2152
state 3	548.58 nm	f = 0.0023	state 4	547.36 nm	f = 0.0020
305 → 309		0.3911	305 → 310		−0.3085
305 → 310		0.1772	306 → 309		−0.3276
306 → 309		0.1760	307 → 311		0.3859
306 → 310		−0.3898	308 → 312		−0.3710
307 → 311		0.2016			
307 → 312		0.1257			
308 → 309		0.1271			
308 → 311		0.1422			
308 → 312		−0.1925			
state 5	520.51 nm	f = 0.0039			
306 → 309		−0.1060			
307 → 309		0.1014			
308 → 309		0.6559			
308 → 312		0.1632			

[a]The calculated energy (in nm) and oscillator strength (f) are provided as well as the molecular orbital composition of the transition

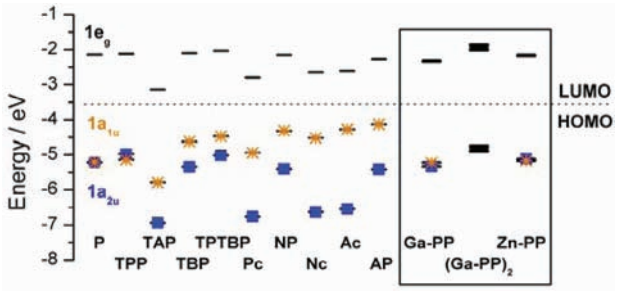

Figure 9. Trends in the energies of the four frontier π-MOs from TD-DFT calculations based on optimizations with 6-31G(d) basis sets. The HOMO symmetries are shown as $1a_{1u}$ (orange star) and $1a_{2u}$ (blue squares) for the symmetric molecules. Adapted from ref 10. Copyright 2005 American Chemical Society The results for Ga-PP, the dimer, and Zn-PP are outlined in the box at the right.

splitting energy of the two top occupied MOs (Δ(HOMO)). The new data fit into the previous trend, extending the data for symmetric porphyrins to the low symmetry PPIX molecule. The significance of this trend is that the new data confirm the spectroscopic analysis that shows very weak Q_{00} bands for both Ga-PP and Zn-PP. A consequence of the low oscillator strength

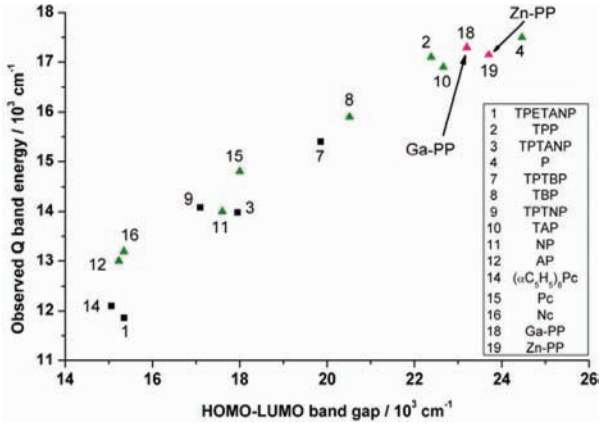

Figure 10. Experimentally observed Q-band energies plotted against the calculated HOMO−LUMO gap from B3LYP calculations with the 6-31(d) basis set. Saddled S_4 or D_{2d} geometry complexes are indicated with a black square. Adapted from ref 10. Copyright 2005 American Chemical Society. The Ga-PP and Zn-PP results are highlighted as pink triangles.

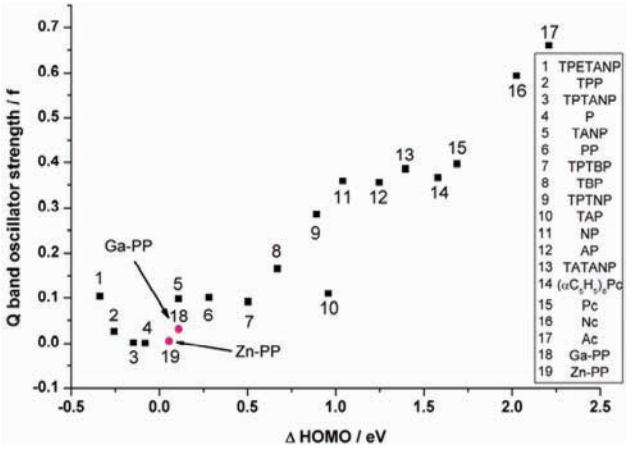

Figure 11. The calculated Q-band oscillator strengths from TD-DFT calculations based on the B3LYP 6-31G(d) basis set plotted against Δ(HOMO). Adapted from ref 10. Copyright 2005 American Chemical Society. The results for Ga-PP and Zn-PP are highlighted (pink circles).

for Q_{00} is the relative magnitude of the vibronic bands and the sensitivity of the absorption envelope to the presence of charge transfer bands between the metal and the ring.

We investigated a third and final trend: the comparison between the observed and calculated energy of Δ(B-Q_{00}) as a function of Δ(HOMO), Figure 12. The value of this trend is in locating the two $\pi-\pi^*$ bands in the spectra of new porphyrins and in predicting the spectral properties of yet to be synthesized rings. For Ga-PP and Zn-PP, we find that the small energy differences between the highest occupied molecular orbitals accounts for the small Q-B separation gap and very low oscillator strength. An important role for this diagram is in accounting for the bias observed in TD-DFT calculations, where the energy of Q_{00} is overestimated. This can be seen in the differences between the observed (squares) and calculated (triangles) where the calculated data are, for many porphyrins, higher. There are a few cases where this is not the case, for example ZnPc.

dx.doi.org/10.1021/ic202731g | Inorg. Chem. 2012, 51, 3743−3753

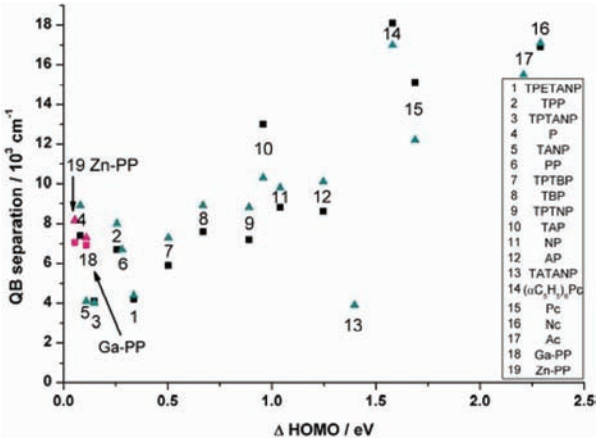

Figure 12. Experimentally observed (black squares) and calculated (green triangles) energy differences between the Q and B bands plotted against ΔHOMO. Adapted from ref 10. Copyright 2005 American Chemical Society. The results obtained for Ga-PP and Zn-PP are highlighted (pink squares for experimental and pink triangles for calculated).

DISCUSSION

Ga(III)protoporphyrin IX (Ga-PP) was suggested as an ideal model for, primarily, the structural properties of ferric hemes because it does not precipitate significantly in solution yet exhibits the trivalent charge absent for Zn(II) porphyrins, the usual choice. The absence of the paramagnetism of the d^5 heme now allows ^{1}H NMR to be used to determine structural parameters. Although Ga-PP has been used in many studies in the past, no definitive optical data have previously been published that establish the precise optical properties. In addition, because of the propensity for aggregation followed by precipitation of ferric hemes, it had been previously thought that Ga(III)PP might also be significantly aggregated, while still maintaining solubility, which would result in a closer model of heme. In this study, we use ESI-mass spectral data to show that the extent of aggregation is small. By introducing the optical data for Zn(II)PP, data not previously reported as far as we can tell, we can compare the data for Ga(III)PP with the comparable data for a main group protoporphyrin IX complex and contrast with the optical data for hemin itself. Our recent development of a trend in optical properties as a function of calculated properties is now extended for the first time to the nonsymmetric protoporphyrin IX ring. The value of these trends is that the theoretical methods commonly used to calculate optical spectra of the porphyrins, TD-DFT and ZINDO/s, usually do not result in an accurate prediction the energies of even the top two states, observed as the Q and B bands. The trends we have previously reported overcome some these issues in part by comparing experimental data to theoretical data. The reported linearity (even if the intercept is not zero) is quite surprising. We now discuss the properties of Ga-PP and the value of each of these experiments to the proposal that Ga-PP can be used as a model for hemin.

Mass Spectral Evidence for the $(Ga\text{-}PP)_2$ Dimer Structure in Solution. The high-resolution mass spectrum (Figure 1) shows that the mass of the dimer in solution corresponds to the calculated mass of the dimer assuming that it forms in a similar manner to that displayed by the hemozoin crystal structure.[7] The crystal structure suggests that the dimer is formed by the propionates at position 6 of the porphyrin ring being involved in the metal coordination. This explains the loss of two protons when comparing the mass of two monomers with the mass of the dimer, as shown below in Scheme 1. The resulting dimer complex is now a neutral species and cannot be seen in a positive mode ESI-MS unless it is protonated in the gas phase (adding 1 Da and one positive charge).

Scheme 1. Effect of Dimerization on the Monoisotopic Mass[a]

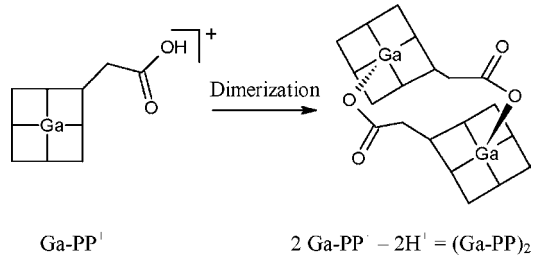

[a]Two protons (and accompanying positive charges) are lost in the formation of the bridging propionates. This is shown in the ESI mass spectrum as the matching mass of the dimer is 1 Da lighter than twice the monomer mass; i.e., 2 times the Ga-PP$^+$ − 2 H$^+$ from bridging propionates + 1H$^+$ for the required positive charge to see it in the ESI-MS in positive mode).

Comparison of the Spectroscopic Data for Ga-PP, Zn-PP, and Ferric Heme. The UV−visible absorption and MCD spectroscopy of Ga-PP and Zn-PP in MeOH are typical of main group porphyrins. The filled 3d shell of the Zn(II) and Ga(III) prevents the large number of charge transfer bands shown in the case of Fe(III) heme so that the B and Q bands can be readily identified. The absence of these charge transfer bands makes interpreting and assigning optical data much simpler and much less arbitrary. Band shifts and ligation status is much more easily recognized in the absence the multiple charge transfer transitions typical of most d-block metals. Of significance is whether the complex electronic structure of heme is an important determinant of the function of heme proteins. Assuming this is the case, the question arises about whether it is solely the Fe(III) metal center or a sum of the Fe(III) and the peripheral groups that are important determinants of the function of heme-containing proteins. Of course, the protein itself is a major determinant, but synthetic models are based on the premise that biologically relevant chemistry can be coaxed from just the heme and its closest substituents.

Ga-PP Insertion into Myoglobin. A key requirement for a model of heme is that the porphyrin will bind to heme proteins. Myoglobin has been used in countless studies to bind a wide range of porphyrins with different metals.[18] The relative intensities of the three species in the ESI mass spectrum indicate that the apo-Mb binds primarily monomeric Ga-PP, with a small fraction left as apo-Mb and another small fraction that binds the dimeric $(Ga\text{-}PP)_2$. This mass spectrum also shows that the free $(Ga\text{-}PP)_2$ dimer coexists with the Ga-PP-Mb in solution, indicating that either the Mb preferentially binds monomeric Ga-PP or that once bound, the Ga-PP forms dimers and precipitates. Comparison of the Zn-PP substituted myoglobin shows band shifts similar to those found in Ga-PP substitution.[19] However, to our knowledge, the only other investigation of Ga-PP binding to heme proteins was recently reported for in vivo production of the catalase enzyme.[9] This group investigated the production of a number of iron-substituted

dx.doi.org/10.1021/ic202731g | Inorg. Chem. 2012, 51, 3743−3753

heme analogues (including Ga-PP and Zn-PP) for their binding to KatA and characterized the substituted enzymes. The UV visible absorption spectroscopy for Ga-PP substituted KatA strongly resembles that of Ga-PP-Mb with a B band at 422 nm and Q bands at 548 and 588 nm. KatA is not as well studied as a model heme binding protein, so inclusion of Ga-PP-Mb binding is valuable as it adds to the already large number of studies of iron-substituted myoglobin examples.

TD-DFT Calculations of Ga-PP. In order to characterize the optical data, the energies and spatial properties of the molecular orbitals were determined using TD-DFT calculations and the excited state transitions for Ga-PP, its dimer, and for Zn-PP examined. The use of zinc as a comparative model is well established[10] as suitable for determining the ring-based components of porphyrin spectroscopy. The lack of charge transfer effects and the absence of the high-spin/low-spin properties (as in the case of other d-block metals such as Fe) simplify the assignment of the optical data. Calculations are also invaluable in that the vibronic overtones that are present in the experimental data are not shown since TD-DFT does not calculate the vibrational bands. To our knowledge, no previous TD-DFT calculations of Zn-PP have been reported, so these data show the effects of solely the ring vs the metal in Ga-PP spectroscopy.

Energy level diagrams were constructed from the TD-DFT calculations for the three molecules. The accidentally degenerate highest occupied MOs and lowest unoccupied MOs are shown in these energy level diagrams (Figure 5 above). We can compare these energy differences to those obtained previously for other Zn porphyrinoids (Figure 9 above). The HOMO splitting for the Ga-PP and its dimer are relatively small compared to the selected representative list of other Zn porphyrinoids. The energy differences between the HOMO and HOMO − 1 are approximately 0.1 eV.

The experimental trends that were established by Mack et al.[10] show how these calculations are useful. Small Δ(HOMO) values are correlated with weaker Q-band oscillator strength (Figure 11) and smaller QB separation (Figure 12). The small Δ(HOMO) difference for the Ga-PP and Ga-PP dimer show that these trends potentially extend to other non-Zn containing porphyrins such as Ga.

The connection of calculated energies to observable properties is also established. It has been demonstrated that larger HOMO−LUMO band gaps are associated with a greater observed Q-band energy. This is due to the fact that the Q-band is generally composed of a high percentage of HOMO−LUMO transition; whereas, the B-band usually involves a large fraction of HOMO − 1 → LUMO and HOMO → LUMO + 1 transitions as well. The Ga-PP and the dimer both follow this trend, which explains why PPIX shows a more red-shifted Q-band than other representative synthetic porphyrins; namely, that the HOMO−LUMO band gap is large and therefore a more red-shifted Q-band is expected and observed.

Finally, the TD-DFT calculations provide the individual molecular orbital surfaces. We can compare both the symmetry and purity of the transitions in order to qualitatively investigate the roles of (i) peripheral substituents on the rings, (ii) the coordinated metal within the ring, and (iii) the metal coordinated ligand effect on molecular orbital shape and symmetry. For example, the highest occupied MO for the Ga-PP is of different symmetry (nominally A_{2u}) than the highest occupied MO of the Zn-PP (nominally A_{1u}). DFT calculations of the heme-enzyme catalase active site have shown that the HOMO for this heme adopts an A_{2u} as well.[20]

It is interesting though that the peripheral substituents of the PPIX ring do have an influence on the HOMO and LUMO of the GaPP and ZnPP. Figure 13 shows that the accidentally

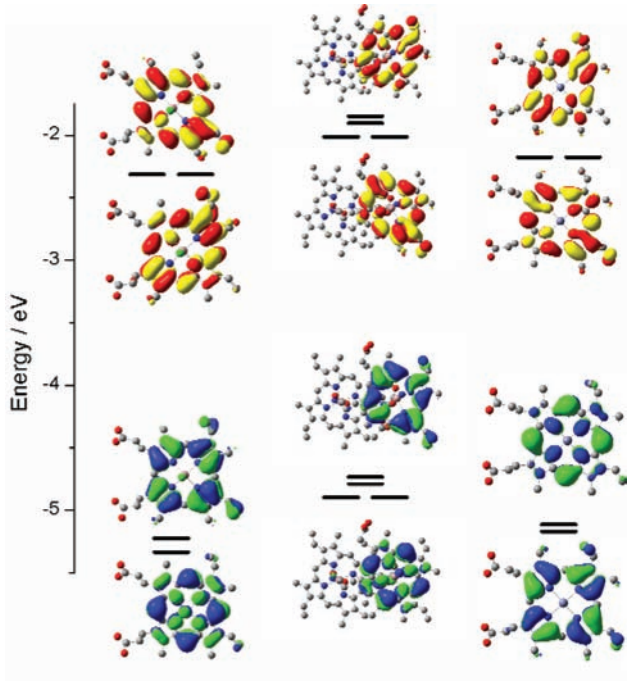

Figure 13. The molecular orbital surfaces of Gouterman's 4-orbitals for Ga-PP-OH, $(Ga\text{-}PP)_2$, and Zn-PP from TD-DFT calculations. The surfaces for the dimer are skewed because of the orientation of the top ring with respect to the bottom ring. Only the MOs for the top ring are shown, as the bottom set mirrors these symmetries.

near-degenerate pairs of the HOMO/HOMO − 1 and LUMO/LUMO + 1 are both distorted when compared with the symmetric MOs calculated for the synthetic porphyrin. The presence of the vinyl and propionic side-chains of the PPIX ring cause shifts in the electron distribution compared to symmetric D_{4h} and D_{2d} porphyrinoids.

CONCLUSIONS

The goal of this work was to investigate the value of Ga-PP as a model for ferric heme. This work demonstrates a multifaceted approach to spectral and theoretical characterization of Ga-PP and also provides a description of how Ga-PP reacts with a heme protein, using myoglobin to illustrate model properties. Through TD-DFT calculation and optical data, Ga-PP has shown to be a suitable mimic of heme and has potential applications in heme replacement/substitution.

We have also shown, through calculated TD-DFT molecular orbitals and energy level diagrams, how the peripheral substituents (the vinyl and propionic side chains) of the protoporphyrin rings are not involved in the main electronic transitions characteristic of metalloprotoporphyrins. The peripheral groups must be much more important when considering the intermolecular porphyrin−porphyrin and especially protein−porphyrin interactions.

dx.doi.org/10.1021/ic202731g | Inorg. Chem. 2012, 51, 3743−3753

AUTHOR INFORMATION

Corresponding Author

*E-mail: Martin.Stillman@uwo.ca.

Notes

The authors declare no competing financial interest.

ACKNOWLEDGMENTS

This work was supported with funding through a CRC to D.S.B., from NSERC to D.S.B. and M.J.S. and the FQRNT (to D.S.B.). We thank Doug Hairsine for ESI-MS technical support and Dr. Viktor Staroverov at the University of Western Ontario for assistance with the TD-DFT calculations.

REFERENCES

(1) Scheidt, W. R.; Reed, C. A. *Chem. Rev. (Washington, DC, U. S.)* **1981**, *81*, 543.

(2) Scheidt, R. W.; Lee, Y. J. Recent advances in the stereochemistry of metallotetrapyrroles. *Metal Complexes with Tetrapyrrole Ligands I in Structure & Bonding;* Springer: Berlin/Heidelberg, 1987; Vol. *64*, pp 1−70.

(3) Gouterman, M. In *The Porphyrins*; Dolphin, D., Ed.; Academic Press: New York, 1978; Vol. *3*.

(4) Begum, K.; Kim, H.-S.; Kumar, V.; Stojiljkovic, I.; Wataya, Y. *Parasitol. Res.* **2003**, *90*, 221.

(5) Stojiljkovic, I.; Kumar, V.; Srinivasan, N. *Mol. Microbiol.* **1999**, *31*, 429.

(6) Yukitake, H.; Naito, M.; Sato, K.; Shoji, M.; Ohara, N.; Yoshimura, M.; Sakai, E.; Nakayama, K. *Microbiol. Immunol.* **2011**, *55*, 141.

(7) Pagola, S.; Stephens, P. W.; Bohle, D. S.; Kosar, A. D.; Madsen, S. K. *Nature* **2000**, *404*, 307.

(8) Reniere, M.; Torres, V.; Skaar, E. *BioMetals* **2007**, *20*, 333.

(9) Brugna, M.; Tasse, L.; Hederstedt, L. *FEBS J.* **2010**, *277*, 2663.

(10) Mack, J.; Asano, Y.; Kobayashi, N.; Stillman, M. J. *J. Am. Chem. Soc.* **2005**, *127*, 17697.

(11) Nakae, Y.; Fukusaki, E.; Kajiyama, S.; Kobayashi, A.; Nakajima, S.; Sakata, I. *J. Photochem. Photobiol., A* **2005**, *172*, 55.

(12) Teale, F. W. J. *Biochim. Biophys. Acta* **1959**, *35*, 543.

(13) Frisch, M. J.; Trucks, G. W.; Schlegel, H. B.; Scuseria, G. E.; Robb, M. A.; Cheeseman, J. R.; Montgomery, J. A.; Vreven, T.; Kudin, K. N.; Burant, J. C.; Millam, J. M.; Iyengar, S. S.; Tomasi, J.; Barone, V.; Mennucci, B.; Cossi, M.; Scalmani, G.; Rega, N.; Petersson, G. A.; Nakatsuji, H.; Hada, M.; Ehara, M.; Toyota, K.; Fukuda, R.; Hasegawa, J.; Ishida, M.; Nakajima, T.; Honda, Y.; Kitao, O.; Nakai, H.; Klene, M.; Li, X.; Knox, J. E.; Hratchian, H. P.; Cross, J. B.; Bakken, V.; Adamo, C.; Jaramillo, J.; Gomperts, R.; Stratmann, R. E.; Yazyev, O.; Austin, A. J.; Cammi, R.; Pomelli, C.; Ochterski, J. W.; Ayala, P. Y.; Morokuma, K.; Voth, G. A.; Salvador, P.; Dannenberg, J. J.; Zakrzewski, V. G.; Dapprich, S.; Daniels, A. D.; Strain, M. C.; Farkas, O.; Malick, D. K.; Rabuck, A. D.; Raghavachari, K.; Foresman, J. B.; Ortiz, J. V.; Cui, Q.; Baboul, A. G.; Clifford, S.; Cioslowski, J.; Stefanov, B. B.; Liu, G.; Liashenko, A.; Piskorz, P.; Komaromi, I.; Martin, R. L.; Fox, D. J.; Keith, T.; Laham, A.; Peng, C. Y.; Nanayakkara, A.; Challacombe, M.; Gill, P. M. W.; Johnson, B.; Chen, W.; Wong, M. W.; Gonzalez, C.; Pople, J. A. *Gaussian 03W Revision-C.02 Version 6*; Gaussian Inc.: Wallingford, CT, 2003.

(14) Feller, D. *J. Comput. Chem.* **1996**, *17*, 1571.

(15) Schuchardt, K. L.; Didier, B. T.; Elsethagen, T.; Sun, L.; Gurumoorthi, V.; Chase, J.; Li, J.; Windus, T. L. *J. Chem. Inf. Model.* **2007**, *47*, 1045.

(16) Hoffman, B. M.; Petering, D. H. *Proc. Natl. Acad. Sci. U.S.A.* **1970**, *67*, 637.

(17) Michl, J. *J. Am. Chem. Soc.* **1978**, *100*, 6801.

(18) Atassi, M. Z. *Biochem. J.* **1967**, *103*, 29.

(19) Takashima, H.; Matsushima, Y.; Araki, Y.; Ito, O.; Tsukahara, K. *J. Biol. Inorg. Chem.* **2008**, *13*, 171.

(20) de Visser, S. P. *Inorg. Chem.* **2006**, *45*, 9551.